Journal of Membrane Science and Research 6 (2020) 30-39

Journal of Membrane Science & Research

journal homepage: www.msrjournal.com

Research Paper

Correlating Physicochemical Properties of Commercial Membranes with CO_2 Absorption Performance in Gas-Liquid Membrane Contactor

Yilin Xu [1,2], Chandresh Malde [3], Rong Wang [2,4,*]

[1] *Interdisciplinary Graduate School, Nanyang Technological University, 50 Nanyang Avenue, Singapore 639798, Singapore*
[2] *Singapore Membrane Technology Centre, Nanyang Environment and Water Research Institute, Nanyang Technological University, 1 Cleantech Loop, Singapore 637141, Singapore*
[3] *Johnson Matthey Technology Centre, Reading RG4 9NH, United Kingdom*
[4] *School of Civil and Environmental Engineering, Nanyang Technological University, 50 Nanyang Avenue, Singapore 639798, Singapore*

Article info

Received 2019-04-29
Revised 2019-08-01
Accepted 2019-08-06
Available online 2019-08-06

Keywords

Gas-liquid membrane contactor
CO_2 absorption
Physicochemical properties
Wetting
Fouling

Highlights

- Physicochemical properties of membranes synergistically affect CO_2 absorption.
- The coupling of wetting and fouling occur in long-term operations using water as absorbent.
- Amine attack greatly affect the membranes' morphology and stability.

Graphical abstract

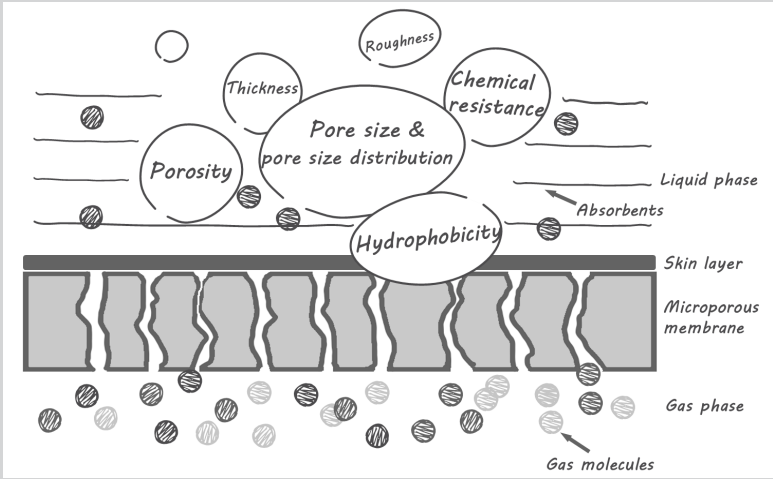

Abstract

The gas-liquid membrane contactor (GLMC) is a promising alternative gas absorption/desorption configuration for effective carbon dioxide (CO_2) capture. The physicochemical properties of membranes may synergistically affect GLMC performances, especially during the long-term operations. In this work, commercial polypropylene (PP) and polyvinylidene fluoride (PVDF) hollow fiber (HF) membranes were applied to explore the effects of their physicochemical properties on long-term CO_2 absorption performances in a bench-scale GLMC rig. PP membranes with pore size of 19 nm, thickness of 0.046 mm, and porosity of 58% achieved high CO_2 flux when feeding pure CO_2 (5.4 and 24.4×10^{-3} mol/m^2.s using absorbents of water and 1M monoethanolamine (MEA), respectively) whereas PVDF membranes with pore size of 24 nm, thickness of 0.343 mm, and porosity of 84% presented a good CO_2 separation performance from the simulated biogas using 1M MEA (6.8×10^{-3} mol/m^2.s and 99.9% CH_4 recovery). When using water as absorbent, the coupled phenomena of membrane wetting and fouling restricted CO_2 transport and resulted in continuous flux loss during the long-term operations. When using MEA as absorbent, both PP and PVDF membranes suffered dramatic flux decline. A series of membrane characterization tests revealed that the morphology, pore size, hydrophobicity, and stability of selected commercial membranes were greatly affected by MEA attack during long-term operations. Therefore, the selection criterion of microporous membranes for high-efficiency and long-term stable CO_2 absorption in GLMC processes was proposed. It is envisioned that this study can shed light on improving existing membrane fabrication procedures and the application of novel membrane surface modification techniques to facilitate practical applications of the GLMC technology.

1. Introduction

The worldwide demand for energy is continuously growing with an estimated 27% rise between 2017 and 2040 [1], which triggers a serious reliance on fossil fuels. Carbon dioxide (CO_2), a by-product of fossil fuel combustion, has been recognized as the major anthropogenic greenhouse gas

* Corresponding author at: Phone: +65 6790 5327, fax: +65 6791 0676
E-mail address: rwang@ntu.edu.sg (R. Wang)

DOI: 10.22079/JMSR.2019.107096.1262

leading to global warming. Carbon capture technology is often regarded to as an effective strategy of CO_2 mitigation [2]. Various processes have since been developed to implement CO_2 capture commercially such as liquid absorption, solid adsorption, and membrane technology [3]. Among them, the gas-liquid membrane contactor (GLMC) has been proposed as a viable alternative gas absorption/desorption configuration to conventional contacting processes largely due to its high contacting area, individual gas/liquid flow, energy efficiency, small plant footprint, and operation flexibility [4]. However, the membrane as the major component in the GLMC process represents an undesirable resistance to mass transfer when membrane wetting and/or fouling occur(s), which in turn could considerably affect the CO_2 absorption efficiency thus restricting its application for long-term operations.

In the GLMC process, the hydrophobic microporous membrane acts as a non-selective interfacial barrier between the gas and liquid streams on either side of the membrane, in which the gas transfers from the bulk gas through the membrane pores then diffuses into the liquid phase followed by physical and/or chemical absorption(s) [5]. Most of the commercial membranes available for the GLMC process are made of hydrophobic polymeric materials such as polypropylene (PP), polyethylene, polytetrafluoroethylene (PTFE), and polyvinylidene fluoride (PVDF) [6-8]. However, their applications for CO_2 absorption are often restricted by wetting and swelling, which typically lead to membrane degradation and poor long-term stability [5]. For example, due to membrane-absorbent interactions, PP membranes are vulnerable to chemical attacks through the continuous contact with aqueous amine solutions, resulting in membrane swelling and a significant change in the surface morphology [9,10]. Similarly, despite possessing high hydrophobicity and strong resistance to chemical attacks, PTFE membranes can inevitably succumb to a reduction in absorption flux and change in surface morphology during long-term operations [11].

The membrane wetting phenomenon is brought about by compounding factors such as membrane structure (*e.g.*, pore size) [12], absorbent properties (*e.g.*, surface tension, corrosivity) [13, 14], and mutual interactions between an absorbent and a membrane (*e.g.*, contact angle, swelling, corrosion) [15,16]. The ability of a membrane to resist wetting is usually characterized by its breakthrough pressure (ΔP), which is determined by the Young-Laplace equation as follows [17]:

$$\Delta P = -2\gamma \cos\theta / r_{max} \quad (1)$$

where γ is the liquid surface tension (N/m); θ is the contact angle of the membrane (°); and r_{max} is the maximum radius of the membrane pores (m). Based on this equation, the wetting-resistant properties of a membrane depends on its hydrophobicity, microstructure, as well as the surface tension of the absorbent solution. Ultimately, membranes used for GLMC applications should possess not only high mass transfer efficiency but also excellent anti-wetting properties and long-term stability [18].

Specifically, the GLMC process is associated with three individual mass transfer coefficients (k_g, k_m, and k_l) in the gas phase boundary layer, the membrane, and the liquid phase boundary layer, respectively [5]. The membrane pores can be classified into three modes: non-wetted, overall-wetted, and partial-wetted. The geometrical structure of the membrane can affect the gas mass transfer in the GLMC process. For the non-wetted mode, the mass transfer coefficient through the membrane depends on diffusivity of the gas in the membrane pores ($D_{g,eff}$), thickness, porosity, and tortuosity. $D_{g,eff}$ is determined by the interactions between individual gas molecules (molecular self-diffusion) as well as gas molecules with the walls of membrane pores (Knudsen diffusion, correlated with membrane pore size) [19]. However, for the overall-wetted mode, the mass transfer coefficient through the membrane would be considerably lower than that of a non-wetted membrane due to its extremely low diffusivity in the liquid phase (D_l, $D_l << D_{g,eff}$). Both theoretical simulations and experimental data have proven that the non-wetted operation mode is always preferred. If liquid partially or completely fills the pores thus wets the membrane, the gas molecules inevitably diffuse into the liquid trapped in the pores, resulting in extra resistance and a dramatic reduction in CO_2 mass transfer. Wang *et al.* [15] reported that the CO_2 flux for a non-wetted membrane contactor was about six times higher than that of an overall-wetted membrane contactor. Rangwala [20] investigated that even marginal wetting (< 2%) could lead to a significant resistance of as high as 60% of the overall mass transfer resistance to diffusion in the hollow fiber (HF) configuration. In a separate study, Kumar *et al.* [21] obtained a positive linear relationship between the breakthrough pressure and the surface tension of different liquid solutions namely monoethanolamine (MEA), diethnolamine, methyldiethanolamine, dimethylethanolamine, and *etc.* This study revealed that low liquid surface tension could result in a lower transmembrane pressure and hence worsen the extent of membrane wetting. Moreover, these amine solutions applied in CO_2 absorption processes are generally highly corrosive [22]. Therefore, the chemical stability of the membrane is paramount for GLMC applications.

Many researchers have hitherto paid attention to improving mass transfer performance as well as enhancing the membrane surface hydrophobicity to prevent wetting by developing novel membrane materials [23, 24], modifying fabrication methods [18, 25], and proceeding with surface modification [26, 27]. Many of the past research works have mainly focused on one or two of the above-mentioned areas. However, CO_2 absorption in the GLMC process can be greatly affected by multiple parameters (*e.g.*, geometrical structures of membranes, membrane materials, liquid absorbents, feed gases, operating conditions, and operating time). Yet, there are insufficient data available in the literature to synthetically assess a certain membrane's applicability. Therefore, in hope of scaling up the GLMC process and moving towards industrialization, systematic studies on CO_2 absorption and long-term performances with realistic mixed-gas feed streams are required.

This work seeks to investigate the effects of physicochemical properties of different commercially available membranes on CO_2 absorption in the GLMC process with the aim to facilitate practical application of the process. Due to their desirable properties such as high hydrophobicity, good mechanical strength, multiple pore sizes and porosities, and high commercialization potentials, PP and PVDF HF membranes with various geometrical structures were selected as membrane contactors. To simulate realistic industrial processes, both pure CO_2 and simulated biogas were used as feed gases whereas water and MEA were chosen as absorbents. Their respective CO_2 absorption performances in the GLMC process corresponding with mass transfer coefficients and resistances were studied. Long-term performances of the individual membranes in terms of CO_2 absorption performance as well as the effects on membrane morphology and chemical stability were also investigated.

2. Experimental

2.1. Materials and chemicals

Commercial PP HF membranes (Celgard® X50 and Edgecross™ K35 are labelled as PP-A and PP-B, respectively) and commercial PVDF HF membranes [28, 29] (two batches with different pore sizes of ~20 and ~100 nm are referred to as PVDF-A and PVDF-B, respectively) were used as membrane contactors in this study. MEA (99%, Sigma-Aldrich) was used to prepare the amine absorbent. Tap water was used as the physical absorbent for CO_2 absorption. Pure CO_2 and biogas (CO_2:CH_4 = 40:60) (Singapore Oxygen Air Liquide Pte Ltd.) were used as feed gases for the GLMC experiments. Deionized (DI) water produced by the Milli-Q system, Millipore, USA was used to prepare aqueous solutions.

2.2. Membrane characterizations

The dimensions of the different HFs were measured by a digital microscope (VHX-500F, Keyence, USA). The mechanical properties of the respective membranes were measured by a Zwick Roell Z0.5 materials testing machine (Germany) [30]. A tensiometer (DCAT11, Data physics, Germany) was used to evaluate the dynamic water contact angle values of the individual membranes [31]. A capillary flow porometer (CFP-1500A, Porous Material Inc., USA) was used for characterizing the pore size and pore size distribution of each membrane, which has been described in detail in a previous work [32]. The overall porosity of a membrane (ε_m) was determined via the gravimetric method using Eq. (2) [33]:

$$\varepsilon_m = 1 - \rho_{membrane}/\rho_{polymer} = 1 - m/\left(V_{membrane}\rho_{polymer}\right) \quad (2)$$

where m is the weight of a dry membrane (kg); $V_{membrane}$ is the volume of the membrane (m^3); and $\rho_{polymer}$ is the density of the polymer material (kg/m^3).

A field emission scanning electron microscope (FE-SEM, JSM-7600F, JEOL, Japan) was employed for observations of the surface morphologies of the relevant membranes. The chemical compositions on the different membrane surfaces were investigated by an X-ray photoelectron spectrometer (XPS, AXIS Supra, Kratos Analytical, UK). The detailed operating procedures can be found in our previous study [34].

2.3. CO_2 absorption experiments

The lab-scale GLMC experimental rig used in this work is shown in Figure 1. Membrane modules were prepared by sealing the desired number of HFs in glass tubes [35]. The properties of each membrane module are summarized in Table 1. Feed gas of pure CO_2 or simulated biogas flowed through the lumen side of the HFs controlled by a mass flow controller (Cole-

Parmer®, USA). The gas flow rates of the inlet and outlet sides were each measured by a digital bubble meter (MesaLabs Bios Defender 510L, Bios DryCal Technology, USA). The liquid absorbent (tap water or 1M MEA) flowed counter-currently over the shell side of the HFs controlled by a digital peristaltic pump (MasterFlex® L/S, USA). A micro gas chromatograph (Micro GC, 6890 Hewlett Packard, TCD, Agilent Technologies, USA) was applied to analyze the concentration of inlet and outlet gases [36].

Table 1
Properties of membrane modules.

Items	PP-A	PP-B	PVDF-A	PVDF-B
Module ID, mm	6.5	6.5	6.5	6.5
Module length, cm	6.3	6.3	6.3	6.3
Fiber ID, mm	0.228	0.186	0.845	0.755
Fiber OD, mm	0.320	0.301	1.531	1.464
Fiber length (effective), cm	4.4	4.4	4.4	4.4
Contact area (effective), cm^2	20.4	20.0	8.5	8.1
Number of fibers, N	46	48	4	4

Note: ID and OD refer to inner diameter and outer diameter, respectively.

The CO_2 absorption flux (J, mol/m^2·s) of a membrane can be calculated by Eq. (3):

$$J = P(Q_{g,in} - Q_{g,out})/(RTA_m) \times 10^3 \quad (3)$$

where $Q_{g,in}$ and $Q_{g,out}$ are the inlet and outlet flow rates of gas (10^{-3} m^3·s^{-1}), respectively; R is the ideal gas constant of 0.083 bar·L/mol·K; T is the operating temperature (298 K); A_m is the membrane surface area (m^2); and P is the operating pressure (~1 bar, no extra pressure).

For the simulated biogas upgrading, the CO_2 molecules were absorbed into the liquid absorbent whereas the majority of the CH_4 molecules that could not be absorbed remained in the retentate stream. Thus, the retentate selectivity represents the gas separation efficiency of the process, which is determined using Eq. (4) [8]:

$$\alpha_{R,(CH_4/CO_2)} = C_{CH_4,R}C_{CO_2,F}/(C_{CO_2,R}C_{CH_4,F}) \quad (4)$$

where $\alpha_{R,\frac{CH_4}{CO_2}}$ represents the retentate selectivity; $C_{CH_4,R}$ and $C_{CH_4,F}$ are the concentrations of CH_4 in the retentate stream and feed stream (mol/mol), respectively; and $C_{CO_2,R}$ and $C_{CO_2,F}$ are the CO_2 concentrations in the retentate stream and feed stream (mol/mol), respectively.

Methane recovery is also an indicator parameter of the biogas upgrading process, which can be calculated by Eq. (5):

$$R = Q_{CH_4,R}/Q_{CH_4,F} \times 100\% \quad (5)$$

where R is the methane recovery; $Q_{CH_4,R}$ and $Q_{CH_4,F}$ are the flow rates of CH_4 in the retentate stream and feed stream (m^3/s), respectively.

2.4. Long-term performances

The CO_2 absorption experiments in the GLMC were carried out periodically to observe the long-term performances of the HF membranes. After running of the GLMC process for 2 h, the absorption experiments were suspended. During the interval, the membrane modules were filled with the absorbent (water or 1M MEA) to ensure that the liquid was constantly in contact with the outer surfaces of the membranes.

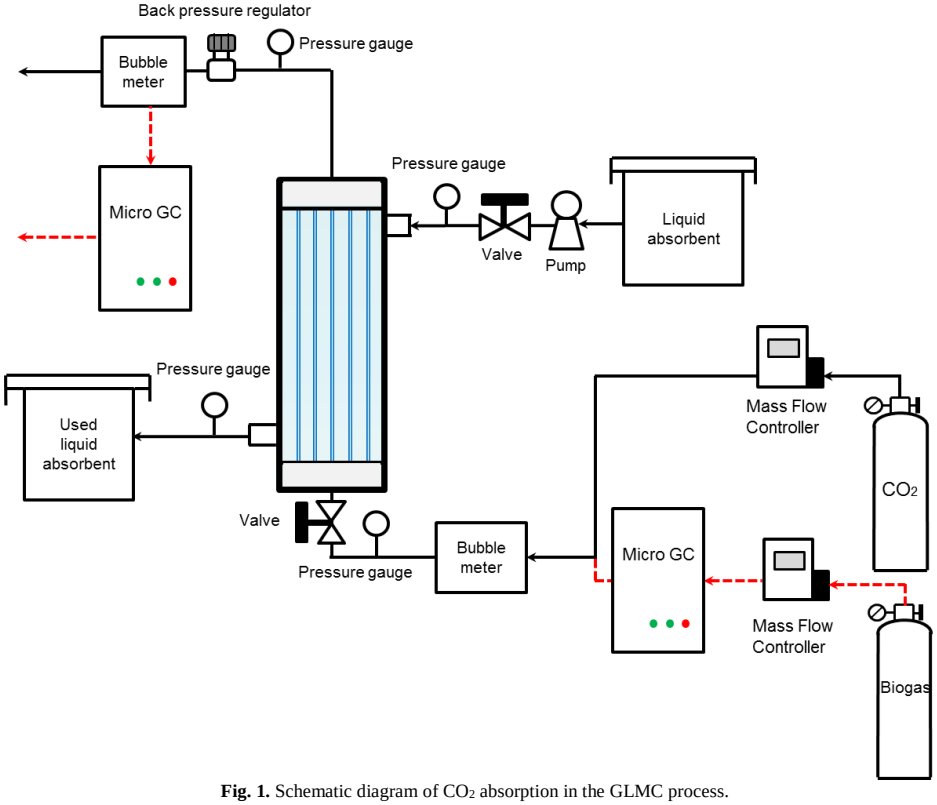

Fig. 1. Schematic diagram of CO_2 absorption in the GLMC process.

The immersion experiments were also carried out to simulate the contacting process for evaluating the physical and chemical stabilities of the commercial membranes. The membrane modules were immersed in 1M MEA solution. The membrane morphologies, pore sizes and pore size distributions, and contact angles were examined periodically.

2.5. Mass transfer of the GLMC

The mass transfer resistances in series of the membrane as well as gas and liquid phase boundary layers can be expressed as follows to describe the mass transfer in a non-wetted GLMC [37]:

$$R_t = 1/K_{ol} = 1/(Ek_l) + Hd_o/(k_m d_{ln}) + Hd_o/(k_g d_i) = R_l + R_m + R_g \quad (6)$$

where K_{ol} is the overall mass transfer coefficient (m/s); E is the enhancement factor; d_o, d_i, and d_{ln} are the outer, inner, and logarithmic mean diameters of the membrane (m), respectively; H is the Henry's law constants (H values for water and 1M MEA solution are 0.831 [12] and 0.665 [38], respectively); R_t is the overall mass transfer resistance (s/m); and R_l, R_m, and R_g are the resistances of the liquid phase, the membrane, and the gas phase (s/m), respectively.

The overall mass transfer coefficient can be calculated by Eq. (7):

$$K_{ol} = Q_l(C_{l,out} - C_{l,in})/(A_m \Delta C_{l,m}) \quad (7)$$

The logarithmic mean concentration, $\Delta C_{l,m}$, can be determined by Eq. (8):

$$\Delta C_{l,m} = \left[\left(HC_{g,in} - C_{l,out}\right) - \left(HC_{g,out} - C_{l,in}\right)\right] / \ln\left[\left(HC_{g,in} - C_{l,out}\right) - \left(HC_{g,out} - C_{l,in}\right)\right] \quad (8)$$

where Q_l represents the liquid flow rate (m^3/s); $C_{l,out}$ and $C_{l,in}$ are CO_2 concentrations of the outlet and inlet in the liquid phase (mol/m^3), respectively; and $C_{g,out}$ and $C_{g,in}$ are CO_2 concentrations of the outlet and inlet in the gas phase (mol/mol), respectively.

Wilson plot is drawn by plotting $1/K_{ol}$ against $1/V^{\alpha}$, where $1/K_{ol}$ can be determined by Eq. (7) and (8). V is the liquid velocity (m/s) and α is the fit value (-0.93) for the liquid absorbent flowing through the shell side of a HF [37]. In the GLMC process, R_g is negligible due to it being much lower than R_t. Therefore, the interception of the Wilson plot represents R_m [12].

3. Results and discussion

3.1. Characterizations of commercial HF membranes

The geometrical structures, dynamic water contact angles, and mechanical properties of PP and PVDF HF membranes were characterized as summarized in Table 2. Commercial PVDF HF membranes were approximately 7 times thicker than the PP HF membranes. The PP-A and PP-B membranes presented similar porosities of around 60% but different pore sizes. The PVDF-A and PVDF-B membranes had much higher porosities of around 85% and quite different pore sizes. By comparing their respective dynamic water contact angles, the PVDF-A membranes possessed higher hydrophobicity as compared to the PVDF-B membranes. As evidenced by their mechanical properties, both commercial PP and PVDF membranes showed enough toughness for GLMC applications.

3.2. CO_2 absorption performance

To investigate the effects of membrane structures on CO_2 absorption performance, the PP-A, PP-B, PVDF-A, and PVDF-B membranes were applied in the GLMC process using water and 1M MEA as absorbents and pure CO_2 as feed gas. As shown in Figure 2(a), CO_2 flux of the PP-A membranes was higher than that of the PP-B membranes, especially when using MEA. This could be ascribed to the lower thickness and smaller pore size with similar porosity of the PP-A membranes, resulting in higher mass transfer coefficient. On the other hand, the larger pore size of the PP-B membranes could lead to higher tendency of pore wetting. For the PVDF membranes, the PVDF-B membranes exhibited lower CO_2 flux in comparison to the PVDF-A membranes (see Figure 2(b)). Since these two PVDF membranes presented similar porosities and thicknesses (Table 2), the differences in CO_2 flux were mainly related to their pore sizes. The larger pore size (~100 nm) of the PVDF-B membranes caused membrane wetting, thus resulting in lower absorption performance. In addition, we observed that the CO_2 fluxes of the PP and PVDF membranes were in a relatively stable or decline trend once the liquid velocity was above 0.25 m/s. This might be due to the large shear force generated by high liquid velocity, which could increase the tendency of membrane wetting. Based on the Young-Laplace equation, liquids with lower surface tension could diffuse more easily into membrane pores. Therefore, the MEA absorbent with lower surface energy aggravated pore wetting for all of the tested membranes.

The Wilson plot method was employed to quantitatively evaluate the mass transfer resistances of the different membranes in the GLMC process (see Figure 3). For the pure CO_2–water system, the membrane mass transfer resistances of the PP-A, PP-B, PVDF-A, and PVDF-B membranes were acquired from the intercept values of the fitted lines on the respective Wilson plots, *i.e.*, 3976, 8044, 4032, and 12542 s/m, respectively. In theory, due to their larger pore sizes, the PP-B and PVDF-B membranes should have presented lower membrane resistances considering their similar structural properties to the PP-A and PVDF-A membranes. However, the obtained mass transfer resistances of the PP-B and PVDF-B membranes were much higher than those of the PP-A and PVDF-A membranes, which could be ascribed to partial-wetting of the pores during the contacting process.

For the pure CO_2–MEA system, the overall mass transfer resistances of the PP-A, PP-B, PVDF-A, and PVDF-B membranes were much lower than those in a pure CO_2–water system because of the higher CO_2 capture capacity of MEA that enhanced the CO_2 absorption efficiency whereas the lower CO_2 solubility of water restricted CO_2 diffusion into the liquid phase. From the fitted lines of the Wilson plots, the resistances of the PP-A, PP-B, PVDF-A, and PVDF-B membranes were 923, 3092, 3332, and 3296 s/m, respectively. At a liquid velocity of 0.25 m/s, the ratios of membrane resistance to total resistance of the PP-A, PP-B, PVDF-A, and PVDF-B membranes were 89%, 95%, 95%, and 81%, respectively. Therefore, the membrane resistance was the main impact factor rather than the mass transfer resistance of the liquid phase, which was in good agreement with previously reported results [39]. When using chemical absorbents, the reduction in membrane resistance should be considered in order to achieve highly efficient CO_2 absorption in GLMC applications. Combining the investigation on CO_2 absorption performances with the analysis of mass transfer resistances, it could be concluded that membrane structures with thinner walls and smaller pore sizes are highly preferred for efficient mass transfer of a single feed gas in the GLMC process.

3.3. Biogas upgrading performance

To further investigate the performance of CO_2 removal from mixed gas in the GLMC process, the PP-A, PP-B, PVDF-A, and PVDF-S membranes were evaluated using simulated biogas as feed gas. Herein, MEA was selected as the absorbent due to its strong CO_2 loading capacity. As shown in Figure 4, the CO_2 fluxes of both the PP and PVDF membranes dropped to 60–70% of their original values in comparison with the pure CO_2–MEA system. This could be attributed to the reduction of CO_2 concentration gradient that led to diminution of the driving force of CO_2 capture. In Figure 4(a), the PP-A membranes exhibited a stable CO_2 flux of around 4.6×10^{-3} $mol/m^2 \cdot s$ under a liquid velocity from 0.10 to 0.30 m/s. However, the flux of CH_4 raised from 1.5 to 1.8×10^{-3} $mol/m^2 \cdot s$. The CH_4 loss of the PP-B membranes was also significant. The results indicated that a severe CH_4 loss occurred in the GLMC process and exacerbated with increased liquid velocity. McLeod *et al.* [40] also verified a significant methane slip (CH_4 loss) during biogas upgrading process in the GLMC using PP HFs. In Figure 4(b), the PVDF-A membranes presented the best separation performance for removing CO_2 from biogas, of which the CO_2 flux reached the highest value of 6.9×10^{-3} $mol/m^2 \cdot s$ at a liquid velocity of 0.25 m/s while the CH_4 flux maintained at a fairly low value thus guaranteed a high CH_4 recovery. On the other hand, the PVDF-B membranes with larger pore size showed an obvious CH_4 loss and a CO_2 flux drop due to the aggravated pore wetting along with an increase in liquid velocity.

Table 2
Properties of commercial HF membranes.

Items	PP-A	PP-B	PVDF-A	PVDF-B
Thickness (mm)	0.046 ± 0.008	0.058 ± 0.005	0.343 ± 0.017	0.355 ± 0.011
Mean pore size (μm)	0.019	0.033	0.024	0.105
Maximum pore size (μm)	0.035	0.062	0.044	0.157
Overall porosity (%)	58.21 ± 0.65	57.31 ± 2.14	84.4 ± 1.10	86.0 ± 1.97
Dynamic contact angle (°)	103.69 ± 0.83	107.29 ± 0.93	111.17 ± 2.92	98.1 ± 0.20
Tensile modulus (MPa)	172.3 ± 3.43	372.3 ± 4.27	26.20 ± 0.98	23.85 ± 1.76
Tensile stress at break (MPa)	106.0 ± 1.89	114.3 ± 2.95	2.00 ± 0.27	2.06 ± 0.11
Strain at break (%)	150.8 ± 3.21	153.3 ± 3.74	97.40 ± 1.02	90.90 ± 5.27

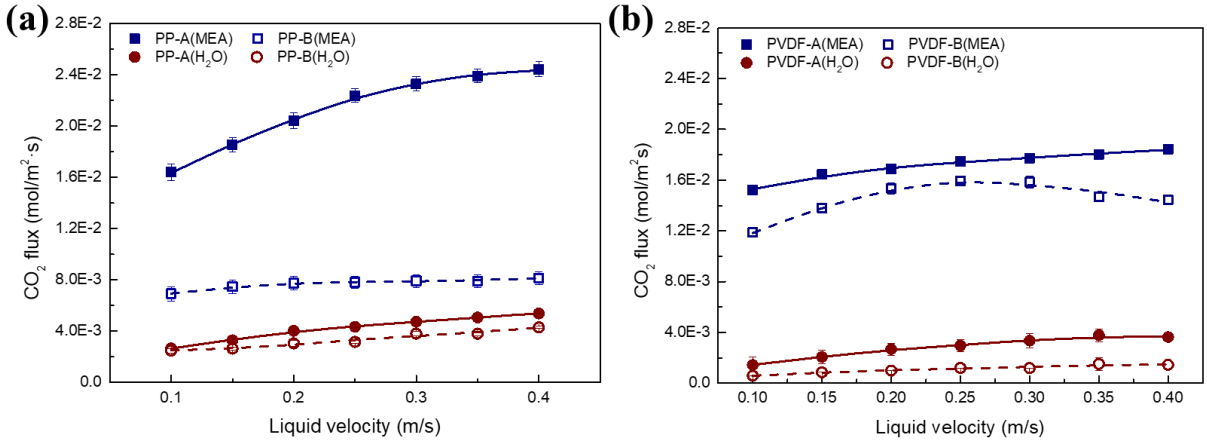

Fig. 2. CO_2 absorption fluxes of HF membranes: (a) PP-A and PP-B, (b) PVDF-A and PVDF-B using MEA and water as absorbents with various liquid velocities.

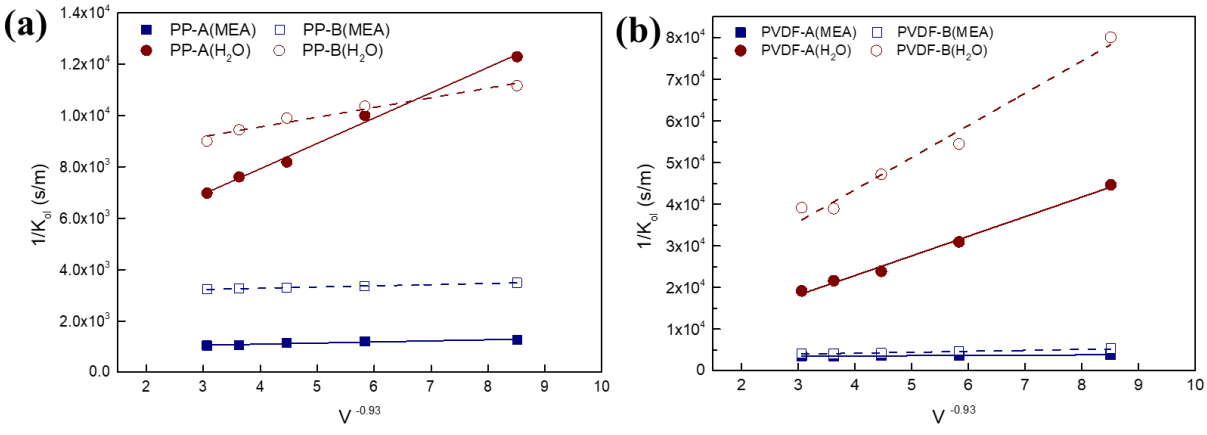

Fig. 3. Wilson plots of commercial membranes: (a) PP-A and PP-B, and (b) PVDF-A and PVDF-B.

As illustrated in Figure 5, the PP and PVDF membranes presented relatively low retentate selectivities with values of less than 2.5. Based on Eq. (4), the selectivity depends on the concentration differences of CO_2 and CH_4 between the inlet and outlet streams, which could be influenced by the membrane surface area, biogas flow rate, and CO_2 loading capacity of the absorbent. Therefore, the lab-scale GLMC setup with limited HF number and module size restricted a high selectivity. Even so, the PVDF membranes showed better retentate selectivity with a value of ~2.0–2.5. The larger porosity of the membranes offered higher gas-liquid contact area and reduced the possibility of pore wetting at the same operation condition, thus restraining the diffusion of CH_4 into the liquid phase. Moreover, the CH_4 recoveries of the PP-A, PP-B, and PVDF-B membranes were around 80–90%, which decreased with increasing liquid velocity accompanied by a deterioration of pore wetting. However, the PVDF-A membranes presented an outstanding CH_4 recovery, approximately 100% at a liquid velocity of 0.30 $m \cdot s^{-1}$. This indicated that almost all of the CH_4 was reserved in the retentate steam of the GLMC process. Therefore, according to investigations of the biogas upgrading flux and analyses of retentate selectivity and CH_4 recovery, we can conclude that membrane structures with smaller pore size and higher porosity would be preferred for highly efficient CO_2 removal from mixed gas.

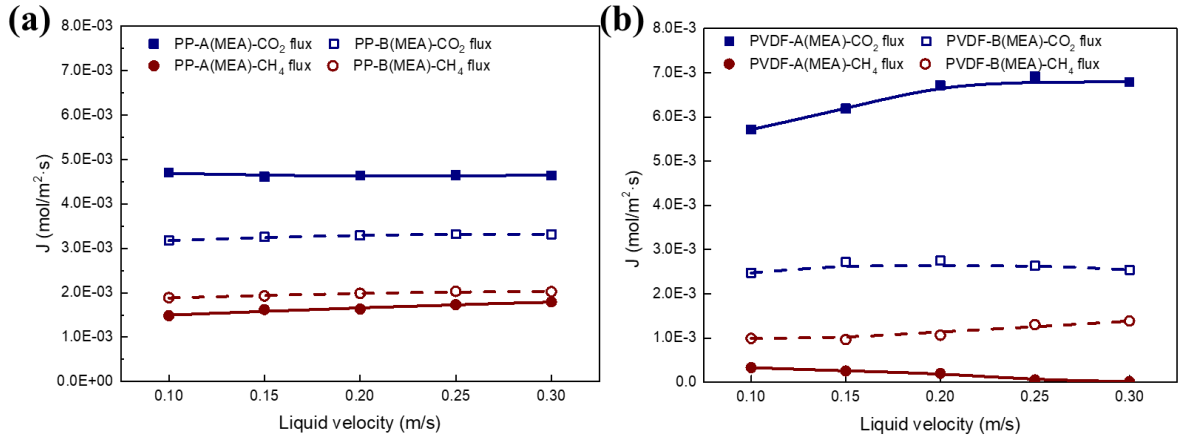

Fig. 4. Gas absorption fluxes (CO_2 flux and CH_4 flux) of commercial membranes: (a) PP-A and PP-B, and (b) PVDF-A and PVDF-B (fed by biogas at a flow rate of 35 ml/min; using 1M MEA absorbent; operated at atmospheric pressure and room temperature of 25℃).

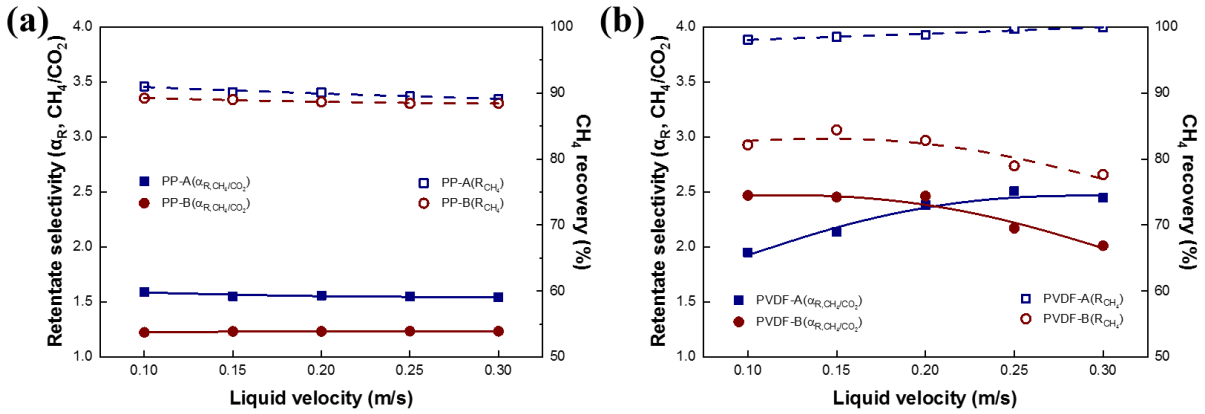

Fig. 5. Retentate selectivities and CH_4 recoveries of commercial membranes: (a) PP-A and PP(B), and (b) PVDF-A and PVDF-B.

3.4. Long-term performance

3.4.1. CO_2 absorption stability

The long-term performances of the PP and PVDF membranes for CO_2 absorption in the GLMC process was evaluated by using physical and chemical absorbents (tap water and 1M MEA). As shown in Figure 6(a), the CO_2 flux of the PVDF-B membranes experienced an obvious slump during the initial 5 days and then gradually decreased to near zero after 32 days of operation. This flux drop could be explained by the low liquid entry pressure contributed by the large pore size of PVDF-B membranes, which induced the onset of pore wetting. Similarly, the PP-A, PP-B, and PVDF-A membranes also suffered pore wetting during the long-term operation, especially during the initial 15 days. In fact, water was able to enter into the pores of the membrane as liquid by capillary action and/or permeation, or as vapor by capillary condensation [41]. With smaller pore size and higher porosity, capillary condensation would be more apparent. Pore wetting of the PP-A, PP-B, and PVDF-A membranes were mainly caused by the capillary condensation phenomenon during the initial long-term operation period. Subsequently, the CO_2 fluxes of the PP-A, PP-B, and PVDF-A membranes exhibited the slow and gradual declines. The surface structures of the PP-A and PVDF-A membranes were further observed by FE-SEM to investigate the possibilities of membrane swelling and membrane fouling (see Figure 7). Organic foulants could be observed on the membrane surface after the long-term GLMC operation, which was attributed to the formation of biological contaminants from tap water. Similar membrane fouling phenomena have also been reported in other works [4, 42]. The foulant layer on the PVDF-A membranes was observed to be denser than that on the PP-A membranes. Moreover, the water contact angle of the PVDF-A membranes revealed a more dramatic change (from 111° to 61°), demonstrating the severity of membrane fouling.

In pure CO_2-MEA system (see Figure 6(b)), the PP-A and PP-B membranes showed dramatic flux drops of 71% and 89%, respectively, throughout a 12-day operation. However, the PVDF-A membranes presented a relatively better performance with only 48% flux drop. Conversely, the PVDF-B membranes showed an obvious flux drop of 81%, mainly due to membrane wetting caused by larger pores. The results revealed that the PP membranes were more sensitive to the MEA solution. Their thinner membrane structure could lead to a higher likelihood of membrane wetting in comparison to the PVDF-A membranes with thicker structure. Moreover, the highly corrosive MEA solution could attack the respective polymer membrane surfaces thus aggravate membrane wetting. Therefore, both the PP and PVDF membranes were degraded over time during long-term operations using amine aqueous absorbent leading to the onset of wetting. Hence, the development of chemical-resistant membranes is necessary to prevent morphology damages and/or swelling problems to realize excellent long-term stability.

3.4.2. Membrane stability

Evaluation of the physicochemical stabilities of the different membranes during contact with chemical absorbents is meaningful for practical applications. Thus, a series of parameters (*e.g.*, morphology, pore structure, and hydrophobicity) for the PP and PVDF membranes after immersing in 1M MEA were characterized in this section to further explore the relationship between the wetting and physicochemical stabilities of the respective membranes. It should be noted that the PP-A and PVDF-A membranes were selected for stability investigation due to their better performances in the previous long-term tests.

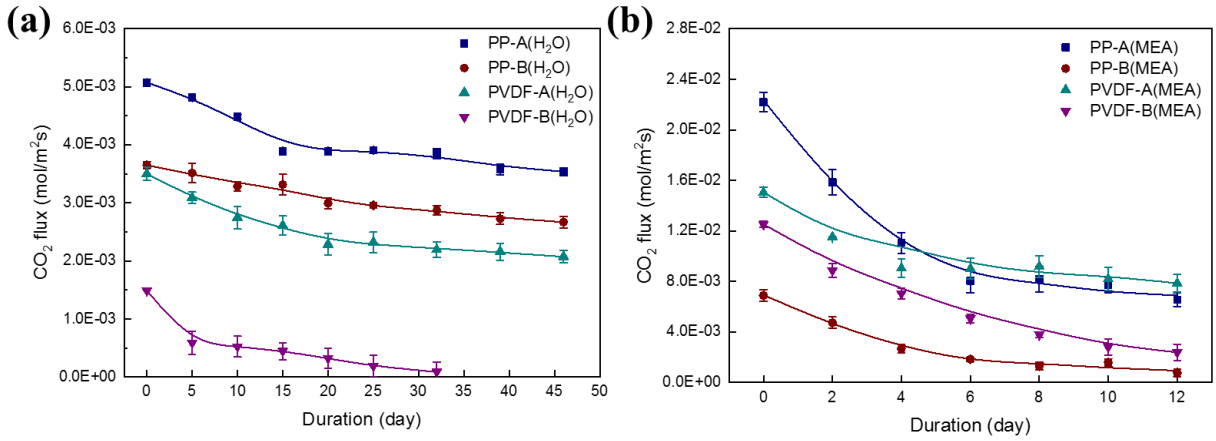

Fig. 6. Long-term performances of the PP-A, PP-B, PVDF-A, and PVDF-B membranes using (a) water (liquid velocity: 0.35 m/s) and (b) 1M MEA as absorbents (liquid velocity: 0.25 m/s).

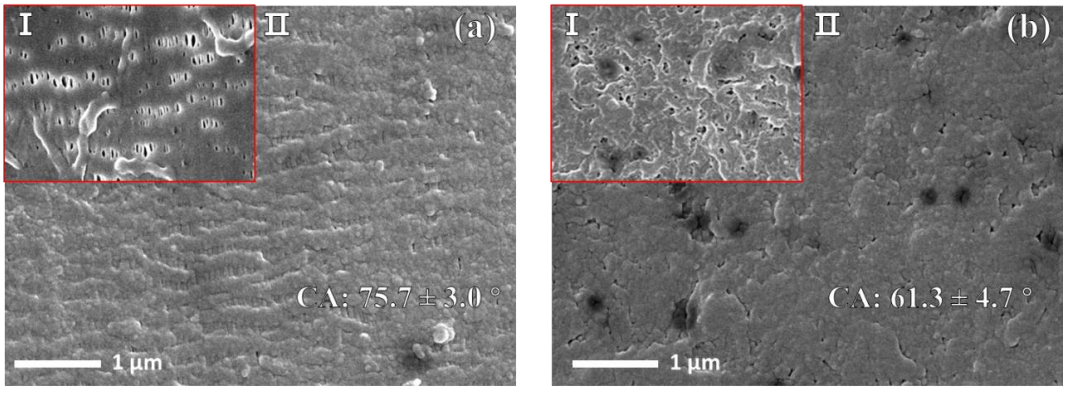

Fig. 7. FE-SEM images (×20.0k) of the outer surfaces of (a) PP-A and (b) PVDF-A membranes: (Ⅰ) original, (Ⅱ) after 46 days long-term operation using tap water as absorbent.

The surface morphologies of the PP-A and PVDF-A membranes after immersing in 1M MEA solution over 1 month were detected by FE-SEM (see Figure 8). Apparent defects and collapsed pore structures could be observed, confirming the chemical attack by the MEA solution. These were the results of the interaction between MEA and membrane materials, which triggered membrane swelling after continuous contact with MEA [9,24].

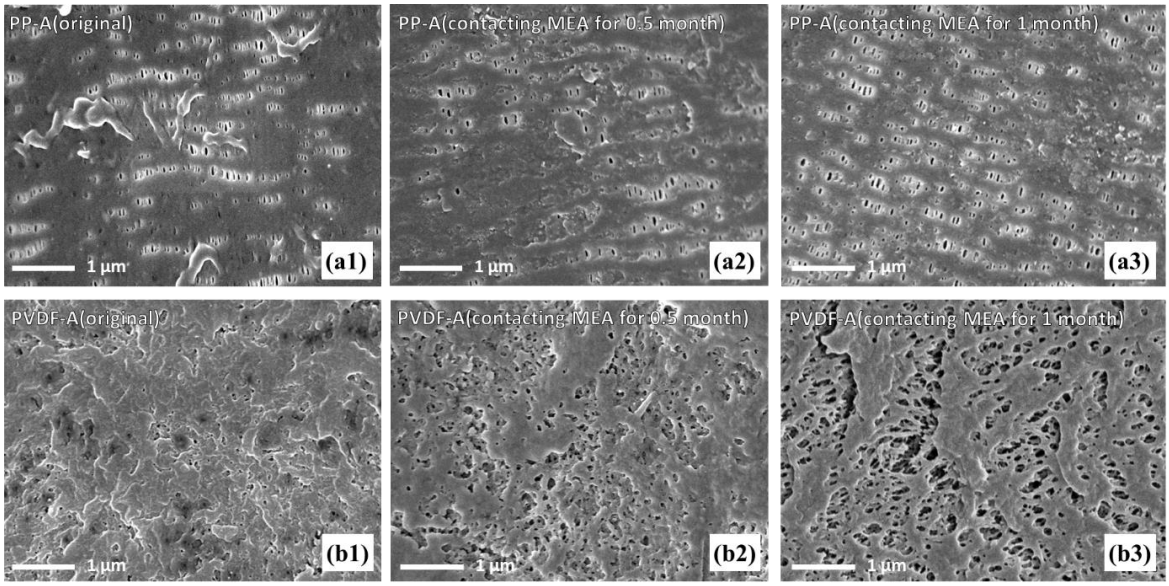

Fig. 8. FE-SEM images (×20.0k) of the outer surfaces of (a) PP-A and (b) PVDF-A membranes: (1) original, (2) after contacting 1M MEA for 0.5 month, and (3) after contacting 1M MEA for 1 month.

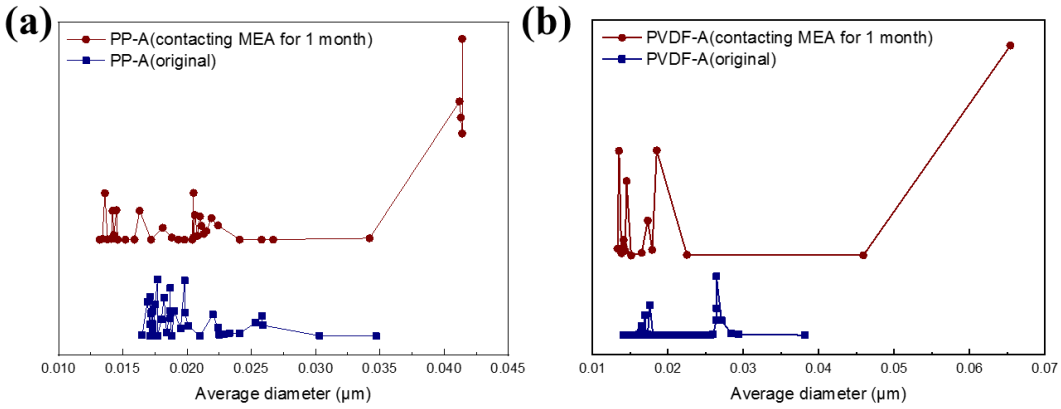

Fig. 9. Membrane pore size distributions after continuous contact with chemical absorbent: (a) PP(A) and (b) PVDF-A membranes.

Moreover, both shrinkage and enlargement of pore structures occurred on the top skin layers of the PP-A and PVDF-A membranes after contacting with MEA for 0.5 month (see Figure 8(a2 and b2)), which could be attributed to the synchronous effects of swelling and MEA erosion on the membrane surfaces. With increasing immersion time, more damages and defects such as fragments and cracks could be observed (see Figure 8(a3 and b3)). Meanwhile, the pore sizes and pore size distributions of PP-A and PVDF-A membranes were examined, as shown in Figure 9. It indicated that a portion of the pores of the PP-A and PVDF-A membranes gathered smaller due to the swelling effect, leading to an increase in membrane resistance. On the contrary, the larger pores could be detected and played the most intensive roles. These defects could render more liquid to stagnate in the pores and accelerate the onset of membrane wetting. Therefore, these changes in membrane morphologies may lead to pore wetting and deterioration of CO_2 transport in the GLMC process, thus compromising long-term operations.

Moreover, the hydrophobicity changes of the PP-A and PVDF-A membranes after exposure to MEA were examined and shown in Figure 10. After contacting with MEA for 1 month, the contact angle of the PVDF-A membranes decreased by 19% from its original value (111°) whereas the contact angle of the PP-A membranes reduced by less than 6%. Sadoogh *et al.* [49] reported that chemical reactions might occur between PVDF and MEA, leading to dehydrofluorination of the polymer. This explains why the reduction in hydrophobicity of the PVDF-A membrane was more severe.

Besides that, the chemical stabilities of the PP-A and PVDF-A membranes after contacting with MEA for 1 month were investigated by analyzing the elemental compositions and chemical bondings of the respective outer membrane surfaces. The elemental compositions from the survey scans of the membranes are listed in Table 3. The contents of the C element of the PP-A membranes and the F and Cl elements of the PVDF-A membranes decreased after erosion by MEA. On the contrary, the contents of the O element of PP-A membranes and the C and O elements of PVDF-A membranes showed significant increasing trends. Meanwhile, the signal of the N element appeared on the surfaces of the PP-A and PVDF-A membranes after contacting with MEA. The results implied that chemical reactions occurred on the PP-A and PVDF-A membrane surfaces. The high-resolution C 1s, O 1s, and N 1s XPS spectra are shown in Figure 11, which further revealed the changes in chemical bonding of the membranes. Compared with pristine membranes, the intensity of the CH_2 of the PP-A membranes after contacting with MEA declined slightly. Conversely, the peaks of C-C, C-H, C-O, O-C=O, and C-N were significantly increased, possibly due to dehydrocarbylation between the PP polymer and MEA. For the PVDF-A membranes, the peaks of CH_2CF_2 and CF_2 of the membranes were weakened after erosion by MEA. On the contrary, the peaks of C-C, C-H, C-O, O-C=O, C-N, and N-H all presented significant enhancements due to dehydrofluorination after amine alkali treatment, which was in good agreement with previous reports [36,43].

3.5. Selection criterion of HF membranes parameters in GLMC processes

Based on the examinations of the CO_2 absorption performance and characterizations of the commercial HF membranes in the GLMC process, we can obtain a basic selection criterion of microporous HF membranes for achieving highly efficient CO_2 absorption and stable long-term performance in different operating conditions as summarized in Table 4. For the various operating conditions, a small pore size with narrow pore size distribution is always the most important property for a hydrophobic microporous membrane used in GLMC for good dispersion of gas into the gas-liquid boundary layer and delay in the onset of pore wetting. However, membranes with a high porosity and a relatively high thickness are preferred for maintaining lower wetting propensity when using the mixed gas as feed gas in the GLMC process.

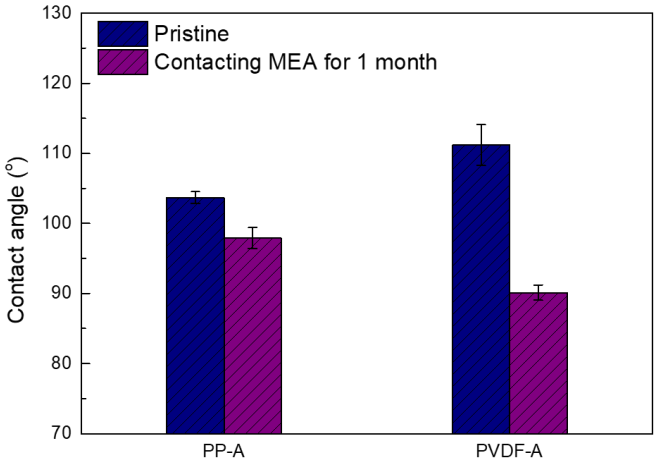

Fig. 10. Hydrophobicities of the PP-A and PVDF-A membranes.

Table 3
Elemental composition of the outer surfaces of the HF membranes.

Membrane	C 1s (%)	F 1s (%)	O 1s (%)	Cl 2p (%)	N 1s (%)
PP-A (original)	91.9	–	8.1	–	–
PP-A (contacting MEA for 1 month)	90.1	–	9.0	–	0.6
PVDF-A (original)	52.4	32.1	1.0	14.5	–
PVDF-A (contacting MEA for 1 month)	54.7	27.5	4.0	12.8	1.1

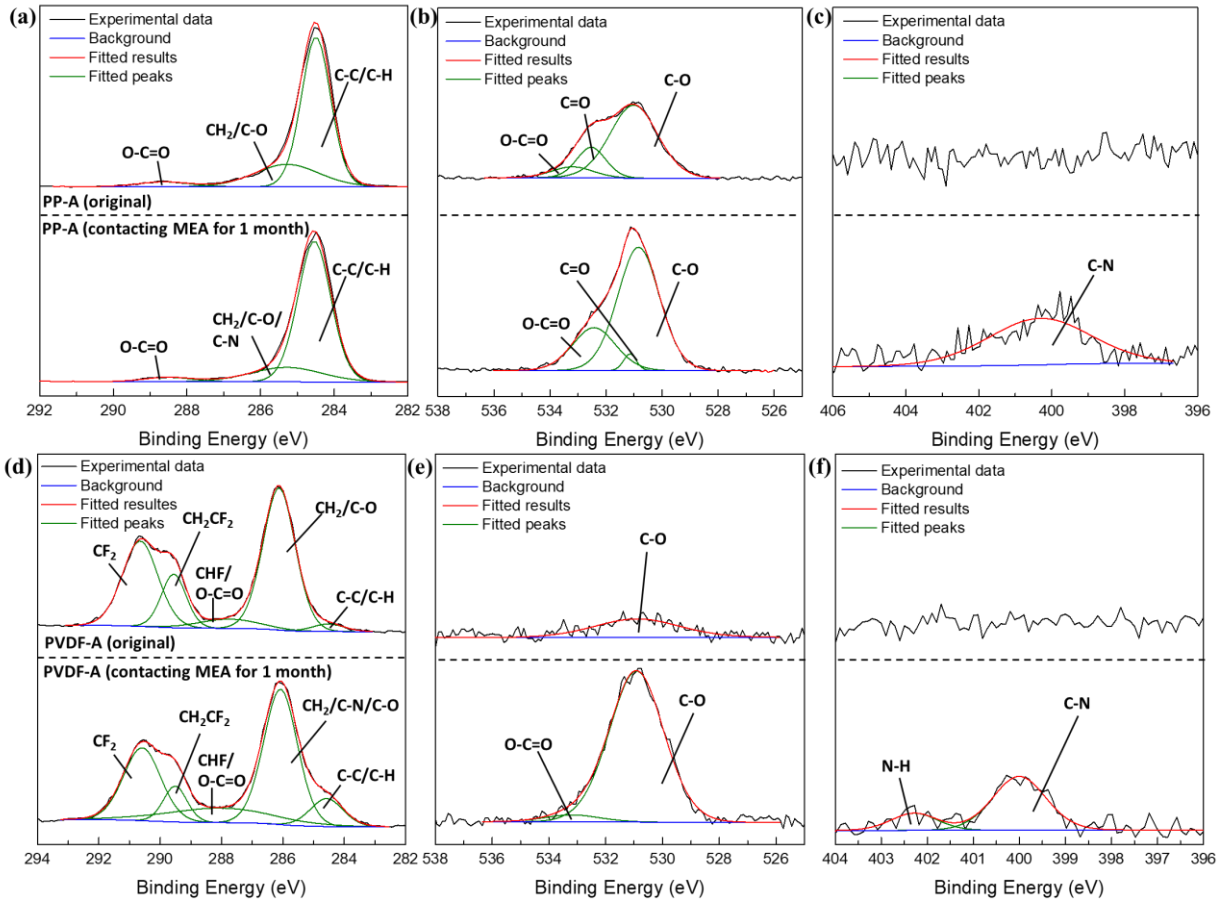

Fig. 11. High-resolution C 1s, O 1s, and N 1s XPS spectra of the outer surfaces of the PP-A (a-c) and PVDF-A (d-f) membranes.

For processes using water as absorbents, both wetting and fouling problems deserve attention. Therefore, an omniphobic membrane with re-entrant structures has been proposed for achieving superhydrophobicity to resist pore wetting as well as oleophobicity to prevent fouling induced by microorganisms in water [44,45]. For processes using amines as absorbents, the membranes are generally preferred to be highly hydrophobic and chemical-resistant for minimizing pore wetting and enhancing the physicochemical stability of the membranes.

Table 4
Selection criterion of microporous HF membranes for highly efficient and long-term stable CO_2 absorption in GLMC processes.

Membrane properties	Single feed gas	Mixed feed gas	Water as absorbent	Amines as absorbent
Small pore size and narrow pore size distribution	+++++	+++++	+++++	+++++
High porosity	++++	+++++	++++	++++
Thin thickness	++++	++	+++	++
Surface roughness	++	++	+++++	++++
Hydrophobicity	+++++	+++++	+++++	+++++
Chemical resistance	++	+++	++	+++++

Note: "+" represents the impact intensity, and "+++++" means the maximum impact intensity.

4. Conclusions

With the aim to provide guidance on the selection of microporous HF membranes for practical applications of the GLMC process, we investigated the effects of physicochemical properties for commercial PP and PVDF HF membranes on CO_2 absorption in the GLMC process using physical/chemical absorbents fed by single/mixed gas. The PP-A membranes exhibited a high CO_2 flux with pure CO_2 as feed whereas the PVDF-A membranes presented a good CO_2 separation performance from biogas. When using water as absorbent for long-term operations, membrane wetting coupled with fouling restricted the CO_2 mass transfer and resulted in a continuous flux drop. When using MEA as absorbent for long-term operations, all commercial membranes suffered dramatic flux declines. Their surface morphologies, hydrophobicities, and chemical properties were greatly affected by amine attack. The results indicated that commercially available microporous HF membranes with suitable geometrical structures could achieve an ideal CO_2 absorption flux but are unsustainable in long-term operations. Thus, to achieve stable performances using water as absorbent, omniphobic membranes should be developed to prevent wetting and fouling. For chemical absorbents, membranes with small pore size, high porosity, high hydrophobicity, and strong chemical resistance are suitable to resist wetting as well as chemical erosion. Therefore, improving fabrication processes or applying novel surface modification methods should be considered in future works for practical applications of the GLMC technology.

Acknowledgements

This work was funded by the Johnson Matthey Public Limited Company. We also acknowledge funding support from the Singapore Economic Development Board to the Singapore Membrane Technology Centre.

References

[1] I.E. Agency, World Energy Outlook 2018, 2018.

[2] A.J. Ragauskas, The path forward for biofuels and biomaterials, Science 311 (2006) 484-489.

[3] F. Bauer, T. Persson, C. Hulteberg, D. Tamm, Biogas upgrading–technology overview, comparison and perspectives for the future, Biofuel. Bioprod. Bior. 7 (2013) 499-511.

[4] Y. Xu, K. Goh, R. Wang, T.-H. Bae, A review on polymer-based membranes for gas-liquid membrane contacting processes: Current challenges and future direction, Sep. Purif. Technol. (2019) 115791.

[5] Y. Zhang, R. Wang, Gas–liquid membrane contactors for acid gas removal: Recent advances and future challenges, Curr. Opin. Chem. Eng. 2 (2013) 255-262.

[6] H.-Y. Zhang, R. Wang, D.T. Liang, J.H. Tay, Modeling and experimental study of CO_2 absorption in a hollow fiber membrane contactor, J. Membr. Sci. 279 (2006) 301-310.

[7] R. Faiz, M. Fallanza, S. Boributh, R. Jiraratananon, I. Ortiz, K. Li, Long term stability of PTFE and PVDF membrane contactors in the application of propylene/propane separation using $AgNO_3$ solution, Chem. Eng. Sci. 94 (2013) 108-119.

[8] S. Atchariyawut, R. Jiraratananon, R. Wang, Separation of CO_2 from CH_4 by using gas–liquid membrane contacting process, J. Membr. Sci. 304 (2007) 163-172.

[9] Y. Lv, X. Yu, S.-T. Tu, J. Yan, E. Dahlquist, Wetting of polypropylene hollow fiber membrane contactors, J. Membr. Sci. 362 (2010) 444-452.

[10] R. Wang, D.F. Li, C. Zhou, M. Liu, D.T. Liang, Impact of DEA solutions with and without CO_2 loading on porous polypropylene membranes intended for use as contactors, J. Membr. Sci. 229 (2004) 147-157.

[11] H. Tang, Y. Zhang, F. Wang, H. Zhang, Y. Guo, Long-term stability of polytetrafluoroethylene (PTFE) hollow fiber membranes for CO_2 capture, Energ. Fuel. 30 (2016) 492-503.

[12] S. Atchariyawut, C. Feng, R. Wang, R. Jiraratananon, D.T. Liang, Effect of membrane structure on mass-transfer in the membrane gas–liquid contacting process using microporous PVDF hollow fibers, J. Membr. Sci. 285 (2006) 272-281.

[13] J.-L. Li, B.-H. Chen, Review of CO_2 absorption using chemical solvents in hollow fiber membrane contactors, Sep. Purif. Technol. 41 (2005) 109-122.

[14] R. Wang, D.F. Li, D.T. Liang, Modeling of CO_2 capture by three typical amine solutions in hollow fiber membrane contactors, Chem. Eng. Process. 43 (2004) 849-856.

[15] R. Wang, H.Y. Zhang, P.H.M. Feron, D.T. Liang, Influence of membrane wetting on CO_2 capture in microporous hollow fiber membrane contactors, Sep. Purif. Technol. 46 (2005) 33-40.

[16] S. Mosadegh-Sedghi, D. Rodrigue, J. Brisson, M.C. Iliuta, Wetting phenomenon in membrane contactors–causes and prevention, J. Membr. Sci. 452 (2014) 332-353.

[17] A.C.M. Franken, J.A.M. Nolten, M.H.V. Mulder, D. Bargeman, C.A. Smolders, Wetting criteria for the applicability of membrane distillation, J. Membr. Sci. 33 (1987) 315-328.

[18] A. Mansourizadeh, A.F. Ismail, M.S. Abdullah, B.C. Ng, Preparation of polyvinylidene fluoride hollow fiber membranes for CO_2 absorption using phase-inversion promoter additives, J. Membr. Sci. 355 (2010) 200-207.

[19] M. Mavroudi, S.P. Kaldis, G.P. Sakellaropoulos, A study of mass transfer resistance in membrane gas–liquid contacting processes, J. Membr. Sci. 272 (2006) 103-115.

[20] H.A. Rangwala, Absorption of carbon dioxide into aqueous solutions using hollow fiber membrane contactors, J. Membr. Sci. 112 (1996) 229-240.

[21] P.S. Kumar, J.A. Hogendoorn, P.H.M. Feron, G.F. Versteeg, New absorption liquids for the removal of CO_2 from dilute gas streams using membrane contactors, Chem. Eng. Sci. 57 (2002) 1639-1651.

[22] W. Rongwong, R. Jiraratananon, S. Atchariyawut, Experimental study on membrane wetting in gas–liquid membrane contacting process for CO_2 absorption by single and mixed absorbents, Sep. Purif. Technol. 69 (2009) 118-125.

[23] Y. Zhang, R. Wang, S. Yi, L. Setiawan, X. Hu, A.G. Fane, Novel chemical surface modification to enhance hydrophobicity of polyamide-imide (PAI) hollow fiber membranes, J. Membr. Sci. 380 (2011) 241-250.

[24] X. Yu, L. An, J. Yang, S.-T. Tu, J. Yan, CO_2 capture using a superhydrophobic ceramic membrane contactor, J. Membr. Sci. 496 (2015) 1-12.

[25] Y. Zhang, R. Wang, L. Zhang, A.G. Fane, Novel single–step hydrophobic modification of polymeric hollow fiber membranes containing imide groups: Its potential for membrane contactor application, Sep. Purif. Technol. 101 (2012) 76-84.

[26] Y. Zhang, R. Wang, Novel method for incorporating hydrophobic silica nanoparticles on polyetherimide hollow fiber membranes for CO_2 absorption in a gas–liquid membrane contactor, J. Membr. Sci. 452 (2014) 379-389.

[27] S. Wongchitphimon, R. Wang, R. Jiraratananon, L. Shi, C.H. Loh, Effect of polyethylene glycol (PEG) as an additive on the fabrication of polyvinylidene fluoride-co-hexafluropropylene (PVDF-HFP) asymmetric microporous hollow fiber membranes, J. Membr. Sci. 369 (2011) 329-338.

[28] N.G.P. Chew, S. Zhao, C.H. Loh, N. Permogorov, R. Wang, Surfactant effects on water recovery from produced water via direct-contact membrane distillation, J. Membr. Sci. 528 (2017) 126-134.

[29] Y. Xu, X. Li, Y. Lin, C. Malde, R. Wang, Synthesis of ZIF-8 based composite hollow fiber membrane with a dense skin layer for facilitated biogas upgrading in gas-liquid membrane contactor, J. Membr. Sci. 585 (2019) 238-252.

[30] Y. Lin, Y. Xu, C.H. Loh, R. Wang, Development of robust fluorinated TiO_2/PVDF composite hollow fiber membrane for CO_2 capture in gas-liquid membrane contactor, Appl. Surf. Sci. 436 (2018) 670-681.

[31] N.G.P. Chew, S. Zhao, C. Malde, R. Wang, Polyvinylidene fluoride membrane modification via oxidant-induced dopamine polymerization for sustainable direct-contact membrane distillation, J. Membr. Sci. 563 (2018) 31-42.

[32] N.G.P. Chew, S. Zhao, C. Malde, R. Wang, Superoleophobic surface modification for robust membrane distillation performance, J. Membr. Sci. 541 (2017) 162-173.

[33] C.H. Loh, R. Wang, Fabrication of PVDF hollow fiber membranes: Effects of low-concentration Pluronic and spinning conditions, J. Membr. Sci. 466 (2014) 130-141.

[34] X. Li, C. Liu, W. Yin, T.H. Chong, R. Wang, Design and development of layer-by-layer based low-pressure antifouling nanofiltration membrane used for water reclamation, J. Membr. Sci. 584 (2019) 309-323.

[35] Y. Xu, Y. Lin, N.G.P. Chew, C. Malde, R. Wang, Biocatalytic PVDF composite hollow fiber membranes for CO_2 removal in gas-liquid membrane contactor, J. Membr. Sci. 572 (2019) 532-544.

[36] Y. Xu, Y. Lin, M. Lee, C. Malde, R. Wang, Development of low mass–transfer–resistance fluorinated TiO_2–SiO_2/PVDF composite hollow fiber membrane used for biogas upgrading in gas–liquid membrane contactor, J. Membr. Sci. 552 (2018) 253-264.

[37] A. Gabelman, S.-T. Hwang, Hollow fiber membrane contactors, J. Membr. Sci. 159 (1999) 61-61-66.

[38] R. Maceiras, E. Álvarez, M.Á. Cancela, Effect of temperature on carbon dioxide absorption in monoethanolamine solutions, Chem. Eng. J. 138 (2008) 295-300.

[39] S. Atchariyawut, R. Jiraratananon, R. Wang, Mass transfer study and modeling of gas–liquid membrane contacting process by multistage cascade model for CO_2 absorption, Sep. Purif. Technol. 63 (2008) 15-22.

[40] A. McLeod, B. Jefferson, E.J. McAdam, Quantifying the loss of methane through secondary gas mass transport (or 'slip') from a micro-porous membrane contactor applied to biogas upgrading, Water Res. 47 (2013) 3688-3695.

[41] L.R. Fisher, R.A. Gamble, J. Middlehurst, The Kelvin equation and the capillary condensation of water, Nature 290 (1981) 575-576.

[42] W. Rongwong, K. Goh, G.S.M.D.P. Sethunga, T.-H. Bae, Fouling formation in membrane contactors for methane recovery from anaerobic effluents, J. Membr. Sci. 573 (2019) 534-543.

[43] Z. Zheng, Z. Gu, R. Huo, Z. Luo, Superhydrophobic poly(vinylidene fluoride) film fabricated by alkali treatment enhancing chemical bath deposition, Appl. Surf. Sci. 256 (2010) 2061-2065.

[44] X. An, Z. Liu, Y. Hu, Amphiphobic surface modification of electrospun nanofibrous membranes for anti-wetting performance in membrane distillation, Desalination 432 (2018) 23-31.

[45] L.-H. Chen, A. Huang, Y.-R. Chen, C.-H. Chen, C.-C. Hsu, F.-Y. Tsai, K.-L. Tung, Omniphobic membranes for direct contact membrane distillation: Effective deposition of zinc oxide nanoparticles, Desalination 428 (2018) 255-263.